GEM NEWS INTERNATIONAL

Contributing Editors
Gagan Choudhary, *IIGJ-Research & Laboratories Centre, Jaipur, India* (gagan.choudhary@iigjrlc.org)
Christopher M. Breeding, *GIA, Carlsbad* (christopher.breeding@gia.edu)
Guanghai Shi, *School of Gemmology, China University of Geosciences, Beijing* (shigh@cugb.edu.cn)

COLORED STONES AND ORGANIC MATERIALS

Unique Colombian emerald and matrix suite. The author recently examined a unique suite of cabochon stones consisting of emeralds with brown matrix weighing 112.25 carats total (figure 1). This spectacular set is reportedly from the Muzo mine in Colombia. Similar material with matrix has been found in Chivor, but never of comparable quality. The miners decided to cut a matching set of cabochons that could be made into a necklace and a pair of earrings. In 2021, Misael Angel Rodriguez of Colombia brought this unique set to the Tucson gem shows, where it received considerable attention. It was later purchased by Desmond Chan and Davey Thomas of Gem Arts International and submitted to the AGTA Spectrum Awards, receiving honorable mention in 2022. To this day, the author has yet to encounter such a remarkable set of matching emerald with matrix cabochons.

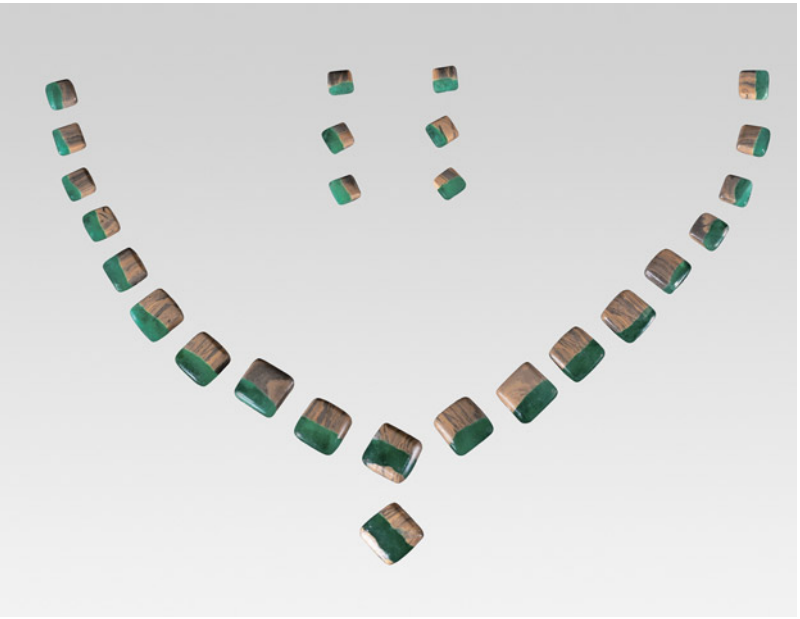

Figure 1. Emerald and matrix suite, 112.25 carats total. Photo by Jessa Rizzo.

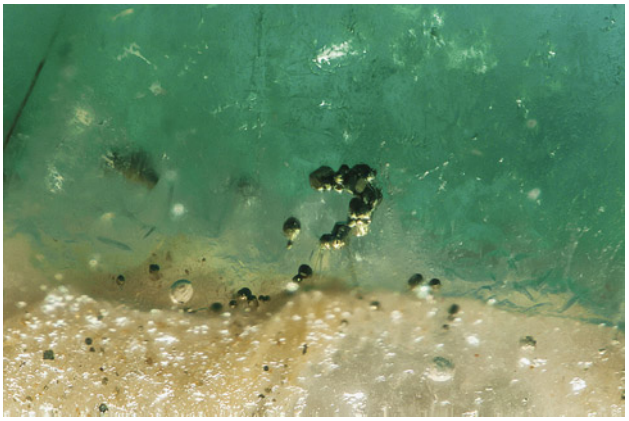

Figure 2. Cluster of pyrite crystals in emerald and matrix. Photomicrograph by Jessa Rizzo; field of view 1.99 mm.

Under the microscope, the matrix has a coarse, sand-like texture. Raman spectroscopy identified the matrix as primarily consisting of an aggregate of feldspar grains displaying a banded pattern. Under magnification, the green gem area showed jagged multiphase inclusions along with euhedral pyrite crystal inclusions (figure 2). Laser ablation–inductively coupled plasma–mass spectrometry and inclusion ob-

Editors' note: Interested contributors should send information and illustrations to Stuart Overlin at soverlin@gia.edu.

Gems & Gemology, Vol. 59, No. 2, pp. 242–260.

Figure 3. The white and cream non-nacreous pearl weighing 0.29 ct and measuring 3.75 × 3.55 mm. Photo by Gaurav Bera.

servation were consistent with a Colombian origin. It is remarkable to see such a well-matched suite of unusual emeralds with matrix in the gem trade.

Jessa Rizzo
GIA, Carlsbad

Calcite present in a pearl from *Pinctada maculata*. *Pinctada maculata* pearls, also known in the trade as "pipi pearls," form in shells considered to be the smallest of all the *Pinctada* species. The shell size ranges from 2 to 6 cm and produces pearls ranging from 1 to 4 mm. However, some rare examples may reach up to 9 mm (Spring 2014 GNI, pp. 89–90). Most pearls from this mollusk exhibit a yellow to "golden" color range, yet some are white to cream, orange, and gray. Round to near-round pearls are quite typical of the species, but other shapes may be found, as with all pearls (N. Nilpetploy et al., "The gemological characteristics of pipi pearls reportedly from *Pinctada maculata*," Winter 2018 *G&G*, pp. 418–427). They are distributed throughout French Polynesia and the Cook Islands and found in shallow waters and depths up to 20 meters. GIA's Mumbai laboratory had the opportunity to examine a quantity of these pearls, which were reportedly sourced from known divers who fished them from wild *P. maculata* mollusks off the Cook Islands. The parcel contained 306 natural pearls of various sizes and shapes, with measurements ranging from 2.87 × 2.69 × 2.55 mm to 8.34 × 3.25 mm.

Real-time microradiography (RTX) showed a variety of internal structures expected for natural pearls. Externally, most samples showed the typical nacreous overlapping aragonite platelets (platy structure) and surfaces that ranged from clean to moderately blemished. However, one near-oval, bicolor white and cream pearl, weighing 0.29 ct and measuring 3.75 × 3.55 mm (figure 3), revealed a very interesting surface structure under 40× magnification. The top part of the pearl exhibited a mosaic, or network of columnar calcite structures in a cellular form (hexagonal and clustered), creating an uneven surface. This was similar to the appearance of non-nacreous pen pearls (N. Sturman et al., "Observations on pearls reportedly from the Pinnidae family (pen pearls)," Fall 2014 *G&G*, pp. 202–215). The bottom part had a combination of both: areas of nacreous overlapping aragonite platelets (the circular ring-like area around the base) and areas of columnar calcite structure (figure 4). The surface was unique among those observed in the lot, as it exhibited both polymorph forms of calcium carbonate (aragonite and calcite). To confirm the non-nacreous cellular areas observed, Raman analysis using a 514 nm laser excitation was carried out on three spots of the pearl's surface (spots 1 and 2 with cellular structure and spot 3 with platy structure). Spots 1 and 2 showed peaks at 280 and 712 cm^{-1}, respectively, indicative of calcite. Spot 3 showed a doublet at 701 and 704 cm^{-1} and a peak at 1085 cm^{-1}, both characteristic features of aragonite (figure 5).

RTX imaging revealed an organic-rich fine acicular feature with no central core, associated with some concentric growth arcs (figure 6, left). X-ray computed microtomography (μ-CT) showed a large central fine acicular feature with a small core showing its calcitic nature, surrounded with thick, dense organic-rich concentric growth arcs (figure 6, right). The internal structure of the pearl matched with the expected columnar structure observed on the surface, as noted in previous research reports.

Energy-dispersive X-ray fluorescence spectrometry revealed a low manganese level of 16 ppm and a higher strontium level of 1286 ppm. Optical X-ray fluorescence was

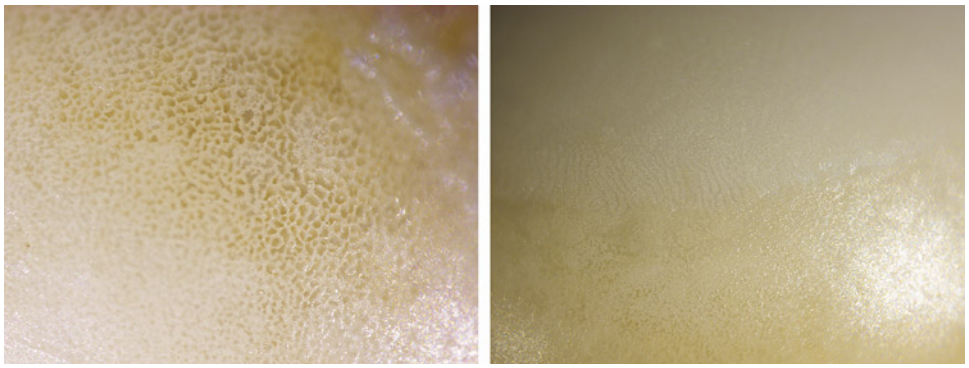

Figure 4. Left: Cellular calcite structure; field of view 0.5 mm. Right: Aragonite platy surface structure; field of view 0.8 mm. Photomicrographs by Pfokreni Nipuni.

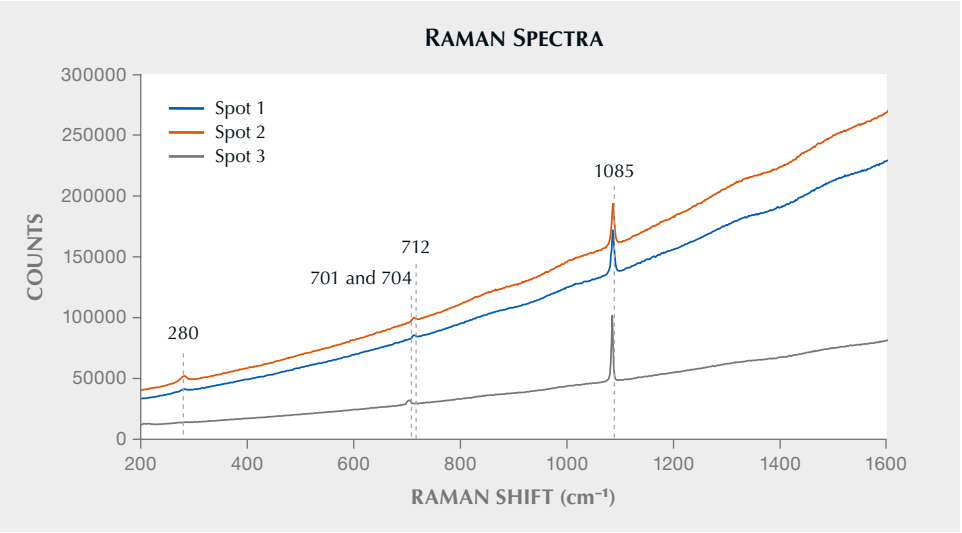

Figure 5. The Raman spectra showed peaks at 280 and 712 cm^{-1} indicative of calcite (spots 1 and 2) and typical aragonite features at 701, 704, and 1085 cm^{-1} (spot 3).

inert, and both results are characteristic of the saltwater environment in which the pearl formed. The pearl showed a moderate bluish green reaction under long-wave UV radiation and a much weaker bluish green reaction under short-wave UV. It was also examined by the ultra-short UV wavelength (230 nm) of the DiamondView, which revealed a clear bluish reaction with fine cellular hexagonal columnar features typically indicative of calcite.

Spectroscopic examination confirmed the presence of both calcite and aragonite. The top and bottom portions of this *P. maculata* pearl exhibited a combination of calcite and aragonite surface features aligned parallel to each other. Such external features are not typically observed in pearls from this mollusk, based on the extensive samples GIA has examined globally, which makes this pearl rare and interesting despite its lack of visual appeal.

Anukul J. Belanke, Roxane Bhot Jain, and Nishka Vaz
GIA, Mumbai

Abeer Al-Alawi
GIA, Global

An unusual metallic core in a natural *Pinctada radiata* pearl from Kuwait. The pearl (oyster) beds, or *heirat* in Arabic, around the State of Kuwait in the Persian (Arabian) Gulf have been known throughout history for producing some of the finest natural pearls. GIA's Bangkok laboratory recently examined a quantity of these pearls obtained from a Kuwaiti pearl diver. The trusted diver said they were fished from wild *Pinctada radiata* mollusks at depths of 6 to 15 meters from one of the main pearl beds in the waters of Kuwait. The parcel consisted of various shapes and colors ranging from white to light yellow, with a few colored pearls as well.

The samples showed a variety of internal structures, but one round cream-colored pearl in particular, weighing 0.23 ct and measuring 3.20 × 3.12 mm (figure 7), revealed an interesting structure using real-time microradiography (RTX) and X-ray computed microtomography (μ-CT) analyses. When viewed under 40× magnification, the pearl's smooth and high-luster surface exhibited typical nacreous overlapping aragonite platelets.

RTX imaging revealed a very unusual small ovalish radiopaque white core located in the pearl's center. The

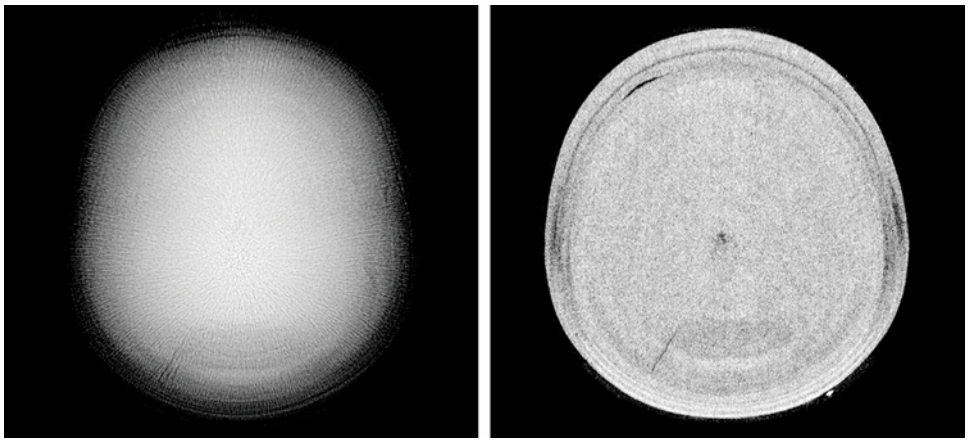

Figure 6. Left: RTX image revealing the calcitic nature of the pearl. Right: μ-CT scans showed a small core with a large acicular structure covering the entire area.

Figure 7. The cream-colored pearl weighing 0.23 ct and measuring 3.20 × 3.12 mm, shown against the anterior of a Pinctada radiata *mollusk. Photo by Nuttapol Kitdee.*

radiopaque core stood out in contrast to the rest of the pearl's structure (figure 8), indicating that the feature was composed of a material containing elements with higher atomic numbers on the periodic table. The appearance of the core was typical of that seen for metals when examined by X-rays, such as the metal post within the drill hole of the pearl in figure 9. The core measured approximately 0.19 × 0.15 × 0.13 mm and was surrounded by fine concentric rings with a small area of associated radiolucent organic-rich material. The small organic-rich area extending toward the outer growth layers appeared darker gray in the RTX and µ-CT images. Although the metallic core created doubts about the pearl's origin, the associated concentric ring structure surrounding it was more indicative of natural origin. The µ-CT scan images were also rendered using specialized software ("New 3-D software expands GIA's pearl identification capabilities," *GIA Research News*, May 13, 2016) to create a three-dimensional image that made it easier to visualize the form of the central metal core (figure 10; see video of the 3D model at www.gia.edu/gems-gemology/summer-2023-gemnews-metallic-core-pinctada-radiata).

Energy-dispersive X-ray fluorescence spectrometry revealed no manganese and a strontium level of 1400 ppm, which is characteristic of a saltwater environment. Raman analysis using 514 nm laser excitation was also carried out on the pearl's surface and showed a doublet at 702 and 705 cm^{-1} as well as a peak at 1085 cm^{-1} indicative of aragonite. Weak polyenic pigment peaks associated with the pearl's cream coloration were also observed at around 1135 and

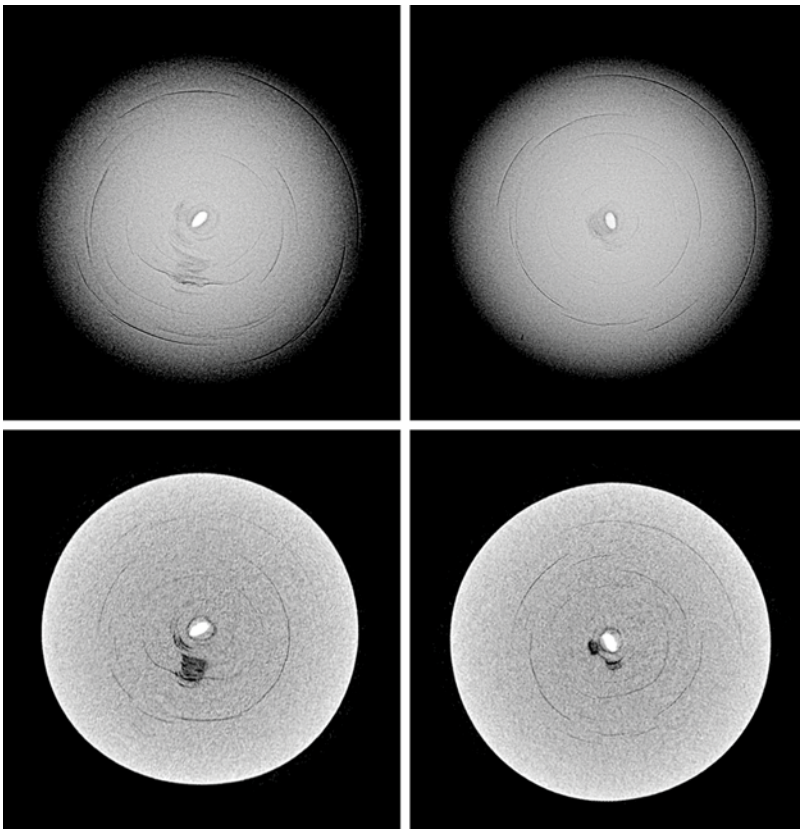

Figure 8. Top: RTX images revealing the entire volume of the pearl's internal structure in two different directions. Bottom: Slightly enlarged µ-CT scans showing the radiopacity of the core more clearly. The darker areas are organic-rich.

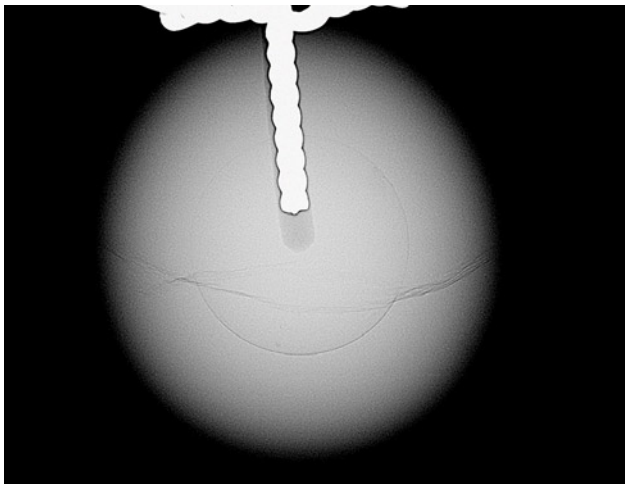

Figure 9. RTX image of a bead cultured pearl reference sample with a metal post in the drill hole. The metal appears radiopaque and matches the appearance of the core feature in the pearl examined in the present study.

1530 cm^{-1}. Ultraviolet/visible reflectance spectra showed features at around 410, 435, and 460 nm and an additional band at 495 nm, in keeping with observations previously recorded for *Pinctada radiata* pearls (A. Al-Alawi et al., "Saltwater cultured pearls from *Pinctada radiata* in Abu Dhabi (United Arab Emirates)," *Journal of Gemmology*, Vol. 37, No. 2, 2020, pp. 164–179).

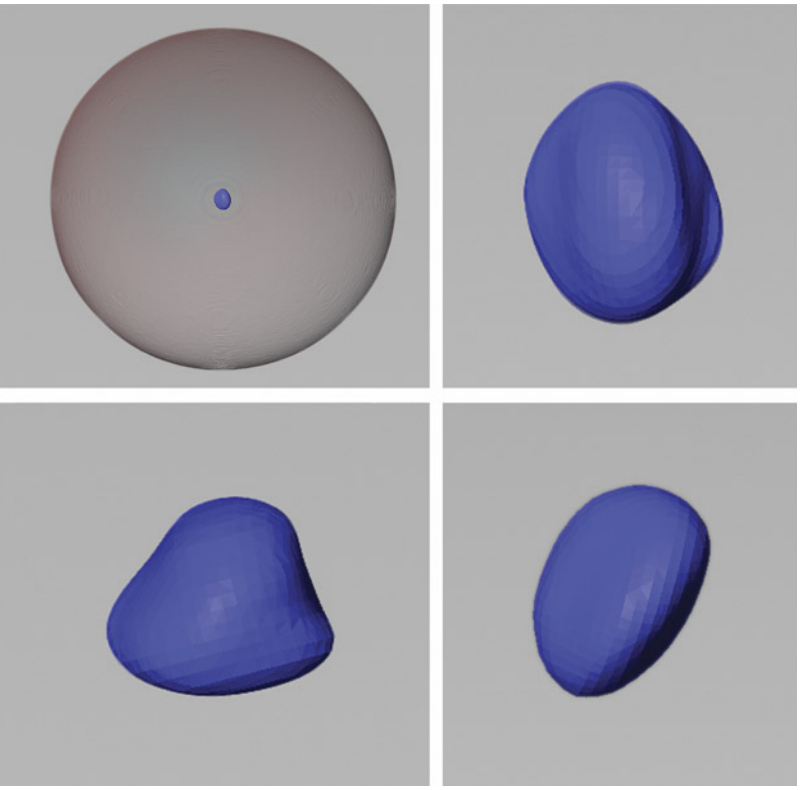

Figure 10. The 3D models generated using µ-CT scans show the blue area as the metallic core, while the surrounding area represents the pearl's growth structure.

Although GIA was not permitted to cut the pearl in half or grind the surface down to reach the metal, we believe the feature may be a metal oxide similar to one previously documented (M.S. Krzemnicki, "Pearl with a strange metal core," *SSEF Facette*, No. 24, 2018, p. 27). How this apparent metal found its way inside the mollusk is still a mystery. Since the diver found the pearl with other natural pearls that GIA also examined and confirmed, and it came from an area that lacks any pearl farms, it seems unlikely that a human inserted the metal core as a bead nucleus. It is possible that the core resulted from the pollution the region witnessed after the Gulf War in 1992, and a foreign metallic particle found its way into a mollusk. Residue from the shipping industry is another possibility, with potential pollution from the heavy volume of oil tankers and other vessels in the area. Hence, water contamination may be a convincing explanation for the unusual structure observed in this unique and fascinating natural Kuwaiti pearl.

Ravenya Atchalak and Kwanreun Lawanwong
GIA, Bangkok

Emiko Yazawa
GIA, New York

Abeer Al-Alawi

Saltwater clamshell beads (*Tridacna* species) used in freshwater cultured pearls. GIA's Bangkok laboratory recently studied 23 intriguing freshwater bead cultured pearls purchased from a vendor in Hong Kong. They displayed an elongated baroque shape with a surface protuberance at one end, and they weighed approximately 20 ct apiece and ranged from 16.73 × 12.58 × 12.49 mm to 18.98 × 13.53 × 13.43 mm (figure 11). Their shape and appearance are similar to saltwater bead cultured pearls known in the market as "Tokki pearls" (A. Homkrajae et al., "Internal structures of known *Pinctada maxima* pearls: Cultured pearls from operated marine mollusks," Fall 2021 *G&G*, pp. 186–205).

Real-time microradiography (RTX) revealed the distinct round demarcation of a bead nucleus with additional void and/or linear features in all the samples, as expected from their external appearance (figure 12, left). However, the beads were more radiopaque and appeared lighter gray in RTX imaging than the traditional freshwater shell bead nuclei widely used in both saltwater and freshwater bead cultured pearl production (P. Southgate and J. Lucas, *The Pearl Oyster*, 2008, p. 286; "Freshwater pearling in Tennessee," *GIA Research News*, October 7, 2016; N. Sturman et al., "Vietnam: Shell nuclei, pearl hatcheries, and pearl farming," Fall 2020 *G&G*, pp. 402–415). Numerous long, thick parasite tubes were visible within the beads,

Figure 11. A strand of baroque-shaped freshwater bead cultured pearls shown with two Tridacna*-species mollusk shells from GIA's shell reference collection. Each sample weighs approximately 20 ct, ranging from 16.73 × 12.58 × 12.49 mm to 18.98 × 13.53 × 13.43 mm. Photo by Nuttapol Kitdee.*

something not often seen in traditional beads (figure 12, right). Optical X-ray fluorescence imaging was used to verify the pearls' freshwater origin. They exhibited weak to moderate yellowish green fluorescence, confirming a freshwater origin. However, the reaction was much weaker than many freshwater bead cultured pearls of the same size and nacre thickness previously examined. These unusual characteristics observed in RTX and X-ray fluorescence imaging led us to cut two pearls in half to investigate the bead nuclei.

The cross sections revealed bead nuclei approximately 12 mm in diameter. The beads appeared chalky white and opaque, unlike traditional beads that are commonly white to cream-colored and semitranslucent. Moreover, the beads exhibited a porcelain-like texture and a subtle flame pattern. We ground the surface of two additional samples to better understand the material. Banded structures of shell formation with subtle flame structures in between were present (figure 13).

Energy-dispersive X-ray fluorescence was used to analyze the elemental concentration of the outer nacre layer and the bead nuclei. The nacre layer showed a high level of manganese and low strontium content, confirming the pearls formed in a freshwater environment. Conversely,

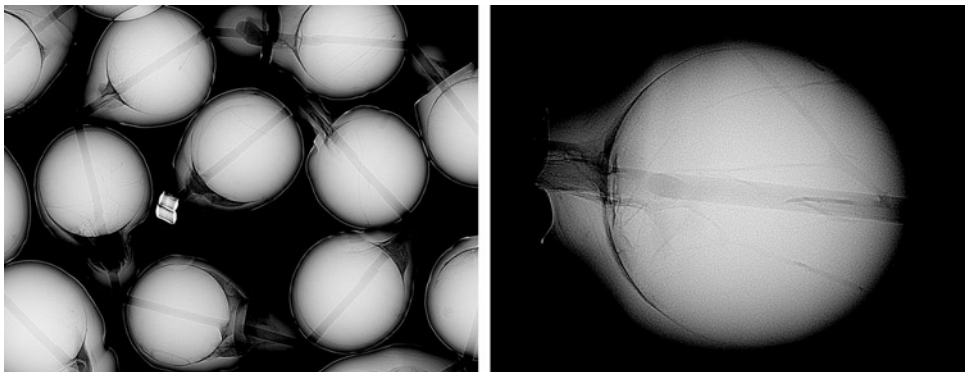

Figure 12. RTX imaging revealed shell bead nuclei approximately 12 mm in diameter entirely covered by the pearl's approximately 1 mm thick nacre (left), with numerous parasite channels in the beads (right).

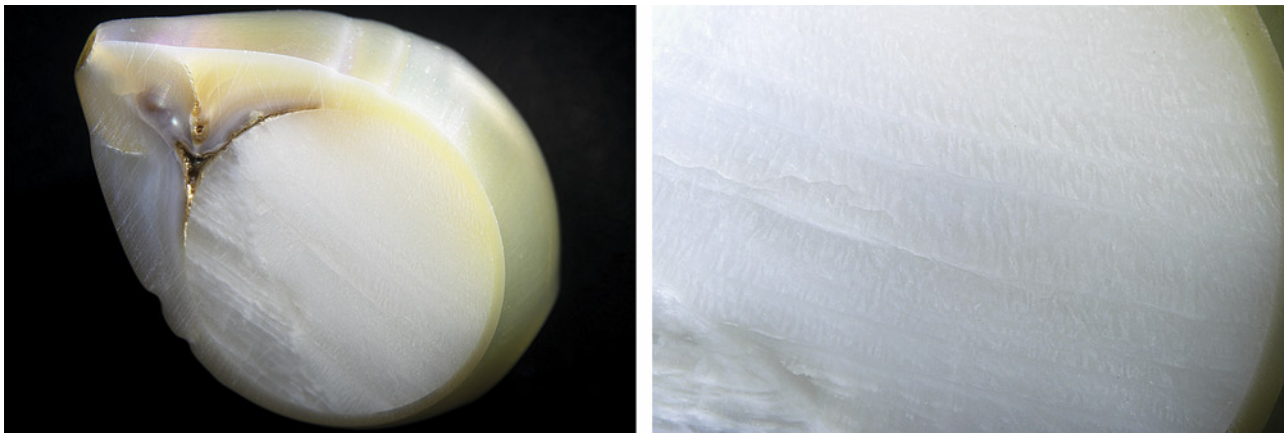

Figure 13. Left: A cross section with the Tridacna *fashioned shell bead nucleus inside showing fine subtle flames in between banded structures. Right: Magnified view of the clamshell bead's flame structure. Photomicrographs by Kwanreun Lawanwong; fields of view 19.20 mm (left) and 7.20 mm (right).*

the bead nuclei showed high strontium (around 1000 ppm) and no manganese was detected, which are typical results for pearls from a saltwater environment. X-ray fluorescence imaging of the cross section displayed a strong yellowish green reaction on the freshwater nacre due to high manganese content, while the saltwater bead nuclei were inert (figure 14). A Raman spectrometer with 514 nm argon-ion laser excitation was employed to analyze the bead nuclei composition, and double peaks at 701 and 705 cm^{-1} and a single peak at 1085 cm^{-1} of aragonite were recorded. Aragonite is a common component of shell and pearl.

The large size, white color, porcelain surface appearance, banded structure with flames, saltwater formation environment, and aragonite composition of the bead nuclei suggested they were created from the clamshell of *Tridacna*-species mollusks. Fashioned shells from *Tridacna* species have been applied particularly in pearl imitations (see Summer 2014 Lab Notes, pp. 153–154; Spring 2015 Lab Notes, pp. 62–63) but are not commonly used in culturing because they are easily broken during the drilling process. More importantly, shells from *Tridacna* species should be avoided for jewelry items or decoration since they are protected by the Convention on International Trade in Endangered Species of Wild Fauna and Flora (CITES), the international agreement that protects endangered species.

Kwanreun Lawanwong

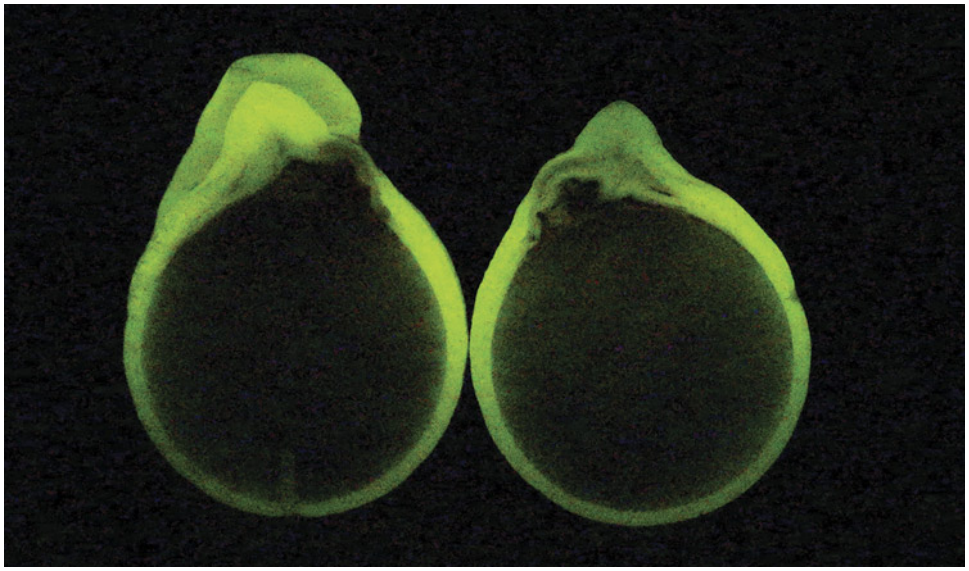

Figure 14. An X-ray illuminated cross section produced a strong yellowish green fluorescence reaction on the freshwater pearl's outermost surface nacre layer, while the inner rounded saltwater clamshell beads showed an inert reaction.

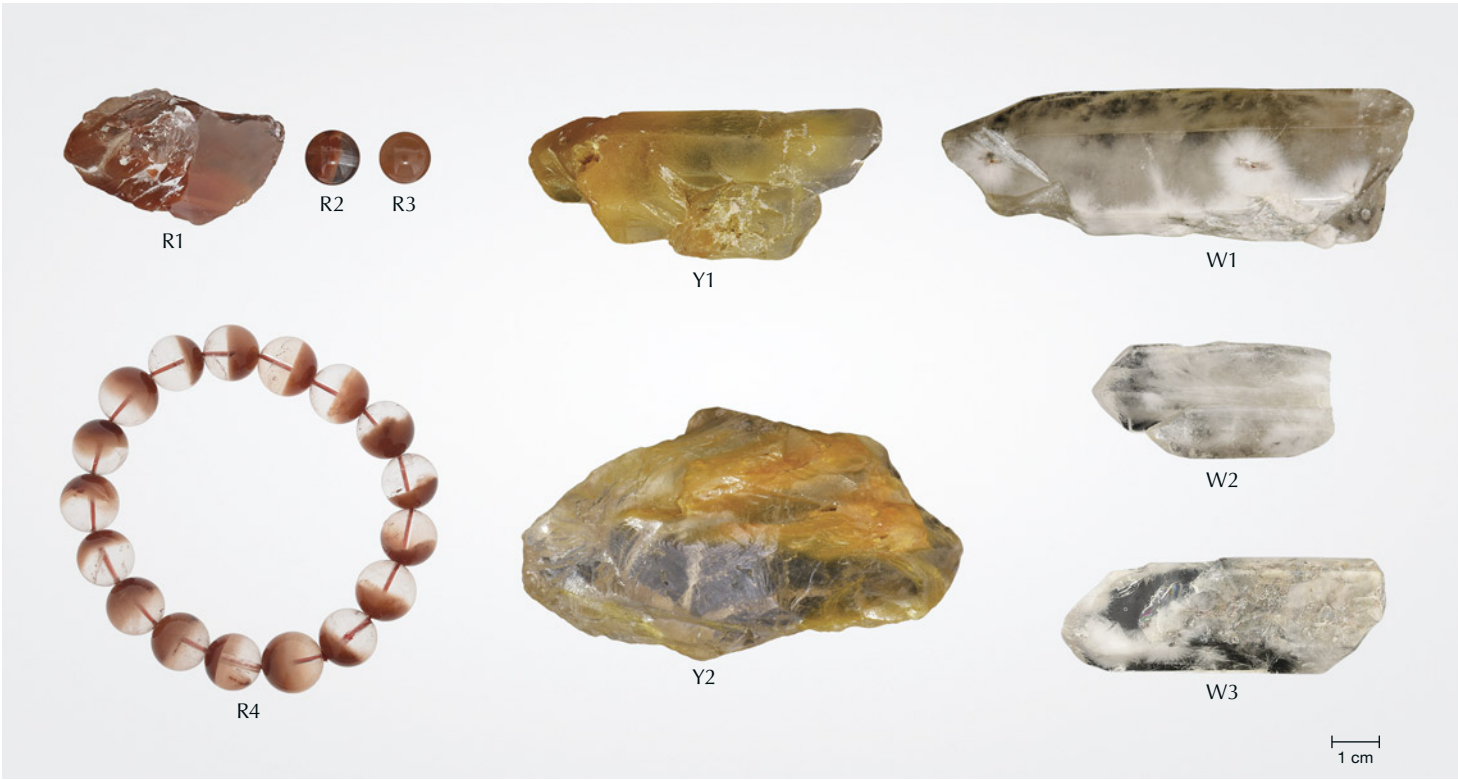

Figure 15. "Rabbit hair" quartz samples with different colors. Photos by Shuqian Rui.

Special hair-like inclusions in quartz. "Rabbit hair" quartz is a commercial variety of quartz with special inclusions. These inclusions resemble rabbit fur and are shorter and thinner than the typical rutile, tourmaline, or other acicular inclusions found in sagenitic quartz. To explore their internal features, nine rabbit hair quartz samples were classified according to the color of their inclusions (figure 15): red (R1–R4), yellow (Y1 and Y2), and white (W1–W3). The white rabbit hair quartz is rarer than the other colors.

Microscopic observation shows slight variation between the different colors of these hair-like inclusions. In the red rabbit hair quartz, massive curved red fibers are distributed evenly. They are mostly brownish red and less than 1 mm in length (figure 16A). The bright yellow needle-like inclusions are distributed regularly but with some localized disorder. Some of the disordered parts form divergent bundles (figure 16B). The white inclusions seem to be hollow tubes, measuring approximately 1–2 mm (figure 16C).

Figure 16. A: Fibrous inclusions in red rabbit hair quartz (sample R1). B: Needle-like inclusions in yellow rabbit hair quartz (sample Y2). C: The tubular inclusions in white rabbit hair quartz (sample W1). Photomicrographs by Shuqian Rui; fields of view 0.71 mm (A), 0.91 mm (B), and 1.26 mm (C).

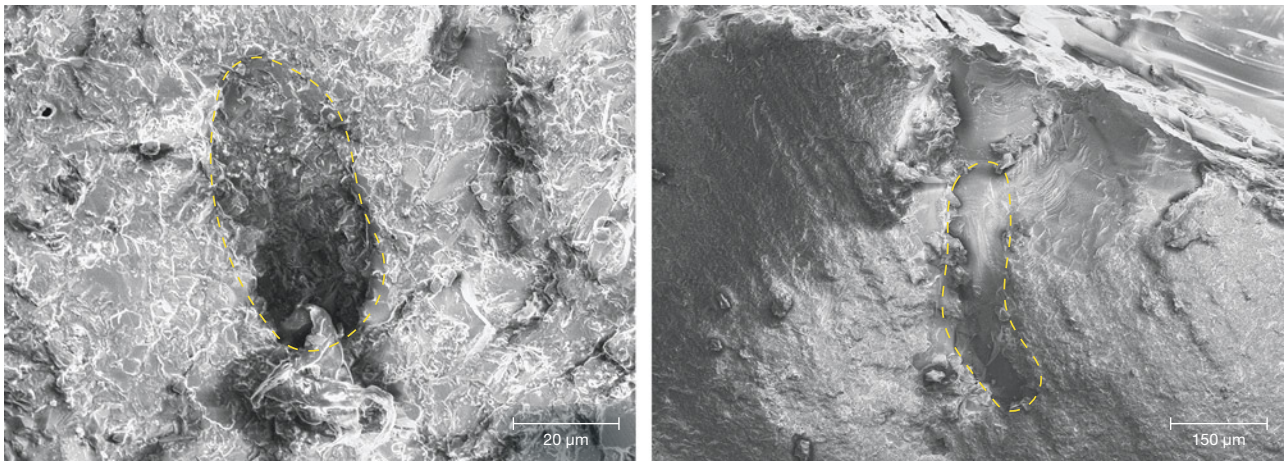

Figure 17. The secondary electron images of the oblique section of the hollow tubes, outlined in yellow (sample W1). Images by Jinyu Zheng.

Raman analysis identified the inclusions in samples W1, R1, and Y2. The hollow tubes in sample W1 with peaks at 208, 266, 355, 405, 465, 810, and 1083 cm^{-1} are the characteristic peaks of quartz. The fibrous red inclusions in sample R1 with peaks at 246, 295, 412, 612, and 1319 cm^{-1} are hematite. The yellow inclusions in sample Y2 with peaks at 305, 394, and 694 cm^{-1} are goethite.

The freshly exposed surface of sample W1 was observed by scanning electron microscope (SEM). Figure 17 shows the secondary electron images; the pits are oblique sections of exposed hollow tubular inclusions (left), and the morphology of parallel sections of hollow tubes can be observed as grooves (right). In the pits, SEM with energy-dispersive spectrometry indicated that the main composition was SiO_2, and no other impurity minerals filled into the hollow.

Fibrous hematite inclusions present in this study are rare in quartz, and their formation is likely related to the growth conditions (I. Sunagawa, *Crystals: Growth, Morphology and Perfection*, Cambridge University Press, Cambridge, 2005, p. 61). White hollow tubular inclusions might be the corroded product of hydrothermal fluids or weathering. In these processes, mineral inclusions were etched away, leaving the hollow tube with its original shape (Winter 2007 GNI, p. 370–373). However, the origin of yellow rabbit hair quartz still needs further research.

Qian Zhang, Shuqian Rui, and Xingtong Li
Gemmological Institute
China University of Geosciences, Wuhan

Jinyu Zheng
School of Earth Sciences
China University of Geosciences, Wuhan

TREATMENTS

Characteristics of treated rubies from Greenland. Rubies and pink sapphire from Greenland are a new addition to the trade. The deposits have been known for decades, but only in the last three years have the finished gems become available in the market. The vast majority of the material is mined by the company Greenland Ruby and disclosed as treated. The habits of the rough corundum crystals are tabular, barrel, or rounded in shape. Their color ranges from dark red to very light pink, with a varying purplish or grayish cast.

Since the stones are mined from a primary deposit, they are often attached to other minerals. Most are mechanically removed at the mine site during the highly automated sorting process. At Greenland Ruby's treatment facility, some stones might be further manually trimmed or clipped to remove more of the matrix. Next, the rubies and pink sapphires are intensely cleaned with strong acids. These dissolve most minerals but do not affect the corundum. Lime is used to neutralize the acid, sometimes leaving a thin white coating on the rough stones.

After cleaning, the stones are heated with flux in crucibles and heated in electric furnaces for multiple hours at high temperatures (>1500°C). This method improves the clarity by healing thin fractures. Excess flux covers the rough stones in a thin glassy layer. After cooling, this product is polished as cabochons or beads. Higher-clarity pieces are faceted. The small amount of corundum produced by artisanal miners is treated in a similar fashion, but their exact procedures are not known.

Inclusion scenes of untreated stones are described in C.P. Smith et al. ("Ruby and pink sapphire from Aappaluttoq, Greenland," *Journal of Gemmology*, Vol. 35, No. 4, 2016, pp. 294–306) and K. Thirangoon ("Ruby and pink sapphire from Aappaluttoq, Greenland: Status of ongoing research," *GIA Research News*, March 23, 2009). These studies highlight the unique and exotic suite of crystal inclusions, including sapphirine and cordierite. We were able to complement these earlier works by studying some of the high-grade material recently produced by Greenland Ruby that has been treated. This is a very intense treatment pro-

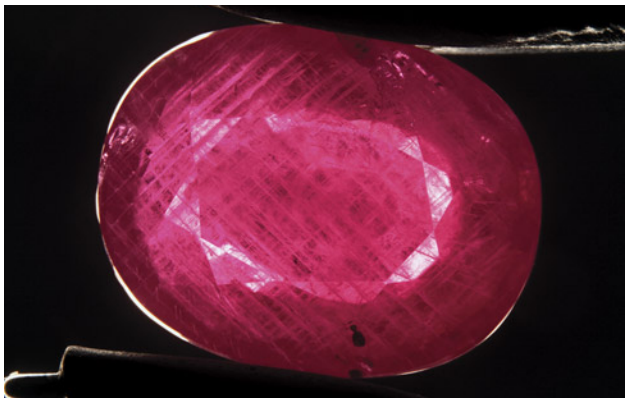

Figure 18. Greenland's rubies are characterized by abundant twinning planes. The twinning planes are not altered by the treatment at a larger scale, but features associated with the twinning can be significantly affected by heating. Photo by S. Wongchacree; field of view 14.40 mm.

cedure that significantly alters the inclusion scenes of Greenland's rubies and pink sapphires.

The most obvious internal features are linked to the omnipresent twinning in corundum from Greenland (figure 18). The twinning planes themselves are not altered by the treatment. The so-called Rose channels, which are hollow tubes at the intersection of twin planes, do show changes. Small fractures, often healed, develop around the linear features, while the tubes themselves usually take on a more spotted appearance when viewed at higher magnification (figure 19A).

Most crystal inclusions show strong alteration, as expected for high-temperature treatment. This makes the unique inclusion scene of Greenland ruby and sapphire unrecognizable. Many of these inclusions transform into "snowballs" with a white frosty opaque nature, often accompanied by discoid fractures that can show signs of healing (figures 19, B and C). In rare cases, crystal inclusions such as zircon remain unaltered.

Less common in Greenland rubies are particles and platelets. Since they require a correct alignment of the observer, platelet, and light source to be detected, they are often overlooked. The particles are a mix of elongated and irregularly shaped platelets. Some could be described as short, stubby needles resembling arrowheads (figure 20, left). They can also appear in dense clouds of finer particles with a roughly hexagonal outline (figure 20, right). These look very similar to the features observed in East African rubies from Mozambique and Madagascar, where they are very common. These seem to be only subtly affected by the treatment. In rare cases, the platelets take a roughly hexagonal form with concentric brightness zoning, resembling a fried egg "sunny-side up." These may be reminiscent of inclusions typically associated with Thai rubies, although Thai rubies almost never show the presence of other particles. We suspect that the unique appearance of these platelets is due to the intense heat they have been subjected to.

Apart from the twinning features, the most obvious features in the treated stones are flux-healed fractures. These are caused entirely by the treatment and are diagnostic of flux healing. As such, they are completely unrelated to a specific origin. Remnants of the flux trapped in the healing fracture can appear as small irregular droplets or connecting worm-like tubes (figure 21, A and B). These might bear some resemblance to natural fingerprints, but they usually have a coarser appearance with more translucent whitish patterns. When the healing is incomplete, the flux can be present in the fractures as a glassy substance showing swirling patterns and trapped gas bubbles (figure 21C).

The treatment has no impact on the corundum's trace element chemistry. The composition of the studied suite is in line with the data reported in Smith et al. (2016). The only values that show some deviation are the titanium concentrations, which are lower in the samples analyzed in this study (12–102 ppmw vs. 81–1227 ppmw in Smith et al.). This might be explained by the higher quality of the samples and thus the absence of cloudy, rutile-rich zones

Figure 19. A: The Rose channels take on a more spotted appearance and can have multiple partially healed fractures around them; field of view 1.44 mm. B: This crystal was completely destroyed; all that remains is a cottony "snowball" inclusion; field of view 1.80 mm. C: All of the inclusions in this cluster developed partially healed fractures around them; field of view 3.60 mm. Photomicrographs by S. Wongchacree (A) and C. Khowpong (B and C).

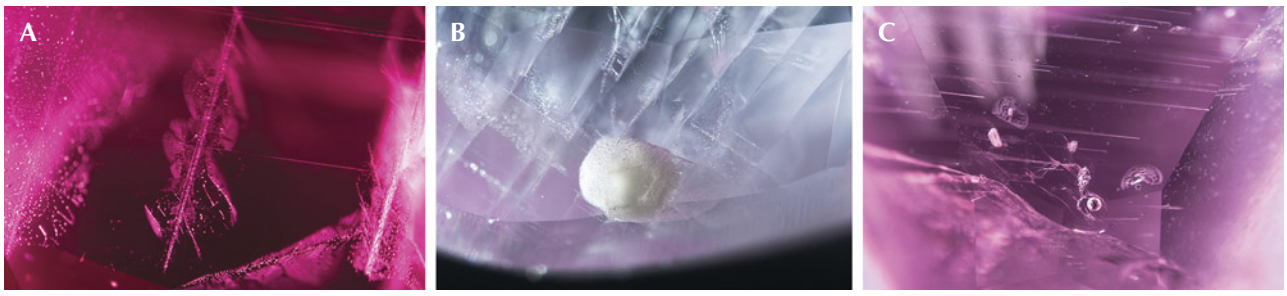

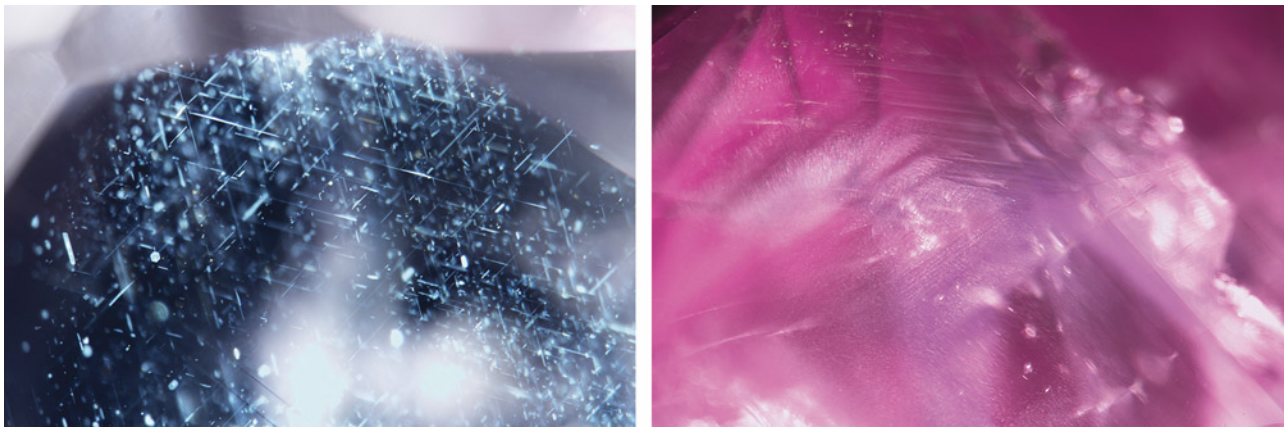

Figure 20. Left: The particles often appear as a mix of short needles, arrowheads, and more irregular shapes. Illuminating them requires the right orientation of the eye, particles, and light source. Right: Dense clouds of finer particles are occasionally found in Greenland rubies. Photomicrographs by C. Khowpong; fields of view 2.40 mm (left) and 2.88 mm (right).

that have higher titanium concentrations. As mentioned in earlier studies, the trace element composition of these stones can overlap with rubies that form in amphibolites, which are commonly encountered in East Africa (mostly Mozambique and Madagascar).

Heat treatment with added flux clearly has a significant impact on the overall appearance and can be easily detected by the multitude of healed fractures. The treatment does alter some important internal features that can complicate origin determination.

Martin Viala
Greenland Ruby, Bangkok
Wim Vertriest, Charuwan Khowpong, and Suwasan Wongchacree
GIA, Bangkok

A new treatment: Creating phantom structure in opal. Phantom structure in opal is a rare and interesting feature found only in Ethiopian opals (www.opalauctions.com/learn/opal-information/phantom-ghost-of-the-opal). The phantom consists of a large spherical inclusion, white and opaque, that is enclosed by transparent, yellow, or colorless host opal—whimsical names include "ghost," "egg," and "mother and daughter" opal. The exotic combination of precious opal surrounded by transparent opal renders this material more attractive and valuable. So far, there has been little research on its characteristics and formation.

At the end of 2021, while performing experiments on natural opal to test changes in transparency and the play-of-color effect with various solutions, the authors accidentally discovered how the phantom formed artificially in natural opal when immersing the stones in a mixture of water, oil, acetone, and other solutions (figure 22). As our curiosity continued to grow, we devised a treatment method to create a phantom in opal by adjusting the amount of solutions, time, and temperature. The phantom opal obtained by the treatment is visually similar to natu-

Figure 21. A: This healed fracture has irregular droplets of flux that were trapped during healing. They stand out due to their high relief and more translucent appearance; field of view 2.88 mm. B: Connecting networks of trapped flux in a healed fracture; field of view 2.80 mm. C: Not all fractures were able to heal to the same degree. Swirling droplets of trapped flux and air reveal that a large portion of this fracture is actually filled with solidified flux rather than healed corundum; field of view 1.20 mm. Photomicrographs by C. Khowpong (A and B) and S. Wongchacree (C).

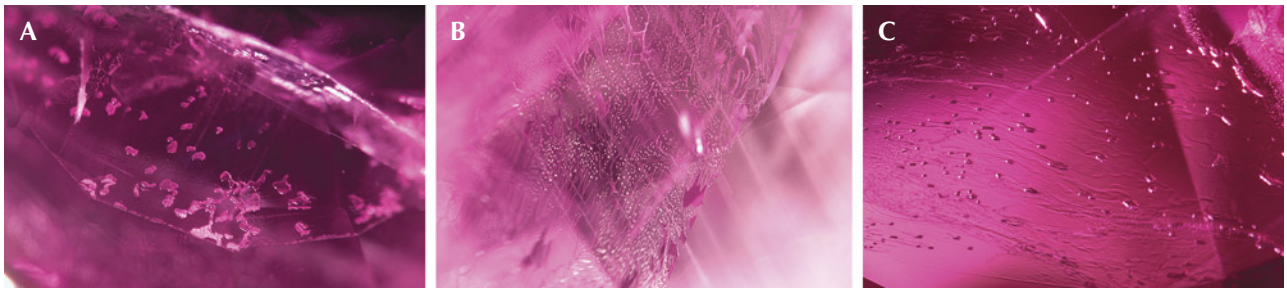

Figure 22. An 11.68 ct treated phantom opal in which the phantom structure appeared during experiments with various solutions. The sample is shown under daylight through the dome (left) and under halogen lighting through the bottom (right). Photos by Le Ngoc Nang.

ral phantom opal (figure 23). The treatment is simple, but it creates a spectacular and bizarre structure that improves the stone's appeal and value.

To reproduce the treatment process, we randomly selected an opal sample purchased from a jewelry store in Ho Chi Minh City (the seller did not know the gem's origin). The oval cabochon weighing 19.0 ct was white in bodycolor and semitranslucent, with weak play-of-color (dull orange, yellow, green, and blue). The gem was tested before and after treatment using standard gemological methods and Fourier-transform infrared (FTIR) spectroscopy with a spectral range from 650 to 4000 cm^{-1} at Liu Gemological Research and Application Center. The refractive index was 1.45 (spot method), and the hydrostatic specific gravity was 1.72–1.85. The stone was inert to long- and short-wave ultraviolet radiation. Examination with a gemological microscope revealed many black inclusions that might be black magnetite. FTIR spectroscopy displayed major absorption bands at 779, 999, and 1638 cm^{-1}. The gemological properties and FTIR analysis indicated natural opal.

After the gemological examination, the opal was soaked in a mixture of 90% vegetable oil and 5% ethanol, and the mixture was boiled at 80°C. Treatment time depended on the sample size and the expected size of the phantom. With longer heating time, more of the "phantom" was converted into transparent opal, resulting in a smaller center and larger surrounding transparent area. In this case, the author decided to treat the gem for 36 hours, and the finished artificial phantom was half the size of the host opal (figure 24). The shape of the phantom was similar to that of the host gemstone. Notably, the play-of-color area shrank after treatment. It went from covering the entire opal to just a thin layer at the outline of the phantom. Interestingly, the dull quality of the play-of-color did improve somewhat.

The characteristics of an opal sample before and after treatment are shown in table 1. Three distinct features can be used to identify the artificial phantom. The first is the morphological similarity between the host opal and its phantom. Second, the treated phantom opal strongly luminesces under long- and short-wave UV radiation as a result of the oil, while the natural opal is usually inert to weak green. Third, the FTIR spectra after treatment exhibit two additional significant peaks at 2853 and 2922 cm^{-1}, attributed to the symmetric and asymmetric stretching vibration of the aliphatic CH_2 group present in oil (N. Vlachos et al., "Applications of Fourier transform-infrared spectroscopy to edible oils," *Analytica Chimica Acta*, Vol. 573–574, 2006, pp. 459–465). The third feature is also the most noticeable evidence that the sample has been treated with oil.

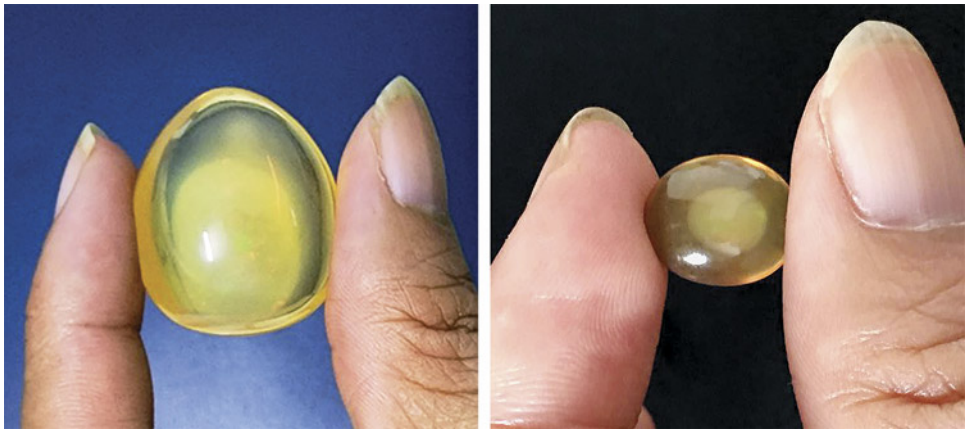

Figure 23. There is no significant visual difference between an untreated Ethiopian natural phantom opal (left, 35 ct) and a treated phantom opal (right, 6 ct). Photos by Le Ngoc Nang.

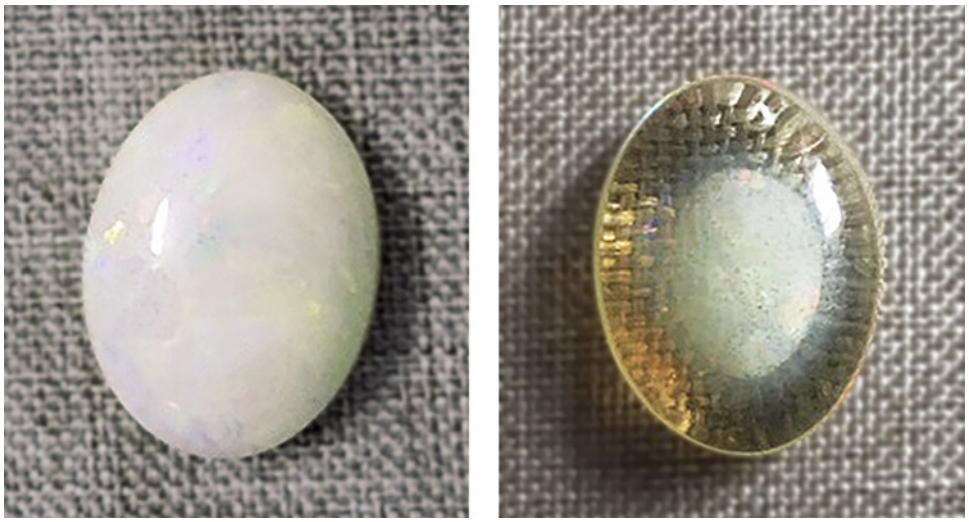

Figure 24. Left: The opal before treatment is semitranslucent white and shows a weak play-of-color. Right: After 36 hours of treatment, the opal becomes transparent light yellow, containing a white phantom. Photos by Le Ngoc Nang.

The treated sample was stored at room temperature under fluorescent lighting for three months to test the treatment's stability. The phantom remained intact, leading the authors to conclude that the treatment stabilization is permanent under normal conditions. The apparent stability of the transparent opal may be explained by the impregnated oil in the stone, which evaporates slowly. To avoid damaging the treatment, however, careful handling is still advised when wearing a stone treated in this way.

In gem trading, treated products must be disclosed. Treated phantom opal may appear commercially in the future, so it is important to disclose our treatment process used to create a phantom structure by impregnating opal with oil and heat, as well as the means to identify the treatment. More importantly, this report is intended to avoid confusion between natural and treated phantom opal.

Le Ngoc Nang and Pham Minh Tien
University of Science, Vietnam National University
Ho Chi Minh City
Liu Gemological Research and Application Center

TABLE 1. Gemological properties of a phantom opal before and after treatment.

Property	Before treatment	After treatment
Weight	9.31 ct	10.06 ct
Bodycolor	White	Yellow
Play-of-color	Weak green-blue-yellow-orange	Medium green-blue-yellow-orange[a]
Shape	Oval	Oval
RI	1.45	1.45
SG	1.72	1.85
Fluorescence	Inert	LW: Strong blue SW: Medium blue
Transparency[b]	Semitranslucent	Transparent
FTIR peaks	782, 1007, and 1645 cm^{-1}	782, 1007, 1645, **2853**, and **2924** cm^{-1}

[a]*The play-of-color on the outline of the phantom*
[b]*The transparency of the host opal*

AUCTION REPORT

Spring 2023 auction highlights. Following a lackluster start to the auction season in Hong Kong, all eyes were on the estate of late Austrian billionaire Heidi Horten in May, presented by Christie's in Geneva. Leading up to the three-part auction, the collection made headlines due to the controversial source of Horten's wealth. (Horten's late husband reportedly made his fortune buying businesses from Jews forced to sell well below value in Nazi Germany.) Despite the controversy, the sale became the most lucrative jewelry auction in history, garnering $202.2 million and surpassing the 2011 auction of Elizabeth Taylor's estate, which totaled $116 million. In accordance with her wishes, proceeds from Horten's estate were donated to a foundation for medical research, child welfare, and access to the arts, while Christie's pledged to donate part of its commission to Holocaust-related charities.

Also in Geneva, Sotheby's rebounded from a disappointing fall 2022 auction season for colored diamonds (Winter 2022 GNI, pp. 524–526) with the sale of the Bulgari Laguna Blu (figure 25). Cut by Bulgari in the 1970s for a private col-

Figure 25. The Bulgari Laguna Blu, an 11.16 ct Fancy Vivid blue diamond, was featured for the first time at auction in Geneva. Courtesy of Sotheby's.

Figure 27. The Estrela de Fura, a 55.22 ct ruby from Mozambique, became the largest and highest-priced ruby ever sold at auction. Courtesy of Sotheby's.

lector, the 11.16 ct Fancy Vivid blue diamond made its auction debut, selling just above its estimate at $25.2 million after only four minutes of bidding. As the highest-priced gem Bulgari has ever sold, the VS_1, type IIb diamond also holds GIA's highest color grade for a blue diamond.

Figure 26. The 126.76 ct Internally Flawless Light of Peace diamond sold for $13.6 million. Courtesy of Christie's.

The season ended on a high note in June with the New York auctions. Leading Christie's Magnificent Jewels sale, the 126.76 ct Internally Flawless Light of Peace diamond (figure 26) was offered without a reserve. Selling within its presale estimate, the GIA-graded type IIa diamond garnered $13.6 million. The largest stone cut from a 435 ct rough unearthed in West Africa, the Light of Peace was once owned by the Zale family, who used the diamond to fund peace-supporting missions. To continue this legacy of goodwill, a portion of the proceeds from the auction will be donated to the United Nations High Commissioner for Refugees.

At Sotheby's Magnificent Jewels auction, two gems smashed multiple records. The Estrela de Fura (figure 27), a 55.22 ct "pigeon's blood" ruby, became both the largest and most expensive ruby ever to sell at auction, raking in $34.8 million. The gem was cut from a 101 ct rough mined in Mozambique in July 2022, which made headlines as the largest gem-quality ruby ever discovered. Remarkable not only for its unprecedented size, the Estrela de Fura's florescence, clarity, and vivid red hue rival that of Burmese rubies. A portion of the proceeds from the sale will help establish the Fura Training Academy in Mozambique, encouraging access for locals to education and technical training in areas such as mining, engineering, carpentry, and agriculture.

Also selling for $34.8 million, the Eternal Pink (figure 28), a 10.57 ct Internally Flawless Fancy Vivid purplish pink diamond, fell just short of its estimate but still surpassed the previous record for a diamond of this color grade. The GIA-graded diamond, which was cut from a 23.78 ct rough from Botswana, set a new record price per

Figure 28. The 10.57 ct Eternal Pink diamond set a new record per-carat price at $3.3 million. Courtesy of Sotheby's.

carat at $3.3 million. Sales of the Eternal Pink and the Estrela de Fura helped Sotheby's break two more records, becoming the first auction to sell two items for more than $30 million each and achieving the highest total ever for a jewelry auction at Sotheby's New York. The overall sale brought in $95.9 million, topping the house's previous record of $65.1 million from April 2015.

Erica Zaidman
GIA, Carlsbad

Figure 29. Susan Jacques accepts the Robert M. Shipley Award at the American Gem Society's 2023 Conclave in Louisville, Kentucky. Courtesy of AGS.

ANNOUNCEMENTS

Susan Jacques receives Robert M. Shipley Award. Susan Jacques, GIA's president and CEO, has received the American Gem Society's Robert M. Shipley Award, honoring her steadfast commitment to the jewelry industry. Named for the founder of GIA and AGS, the prestigious award was presented to Jacques at the AGS Conclave in Louisville, Kentucky, on May 2, 2023 (figure 29).

Jacques previously served as president and CEO of Borsheims in Omaha, Nebraska, one of the nation's largest independent jewelry stores, where she reported directly to Warren Buffett. She served on GIA's Board of Governors beginning in 1996 and held the chair position from 2008 to 2013 before her appointment as president and CEO in 2014. Jacques holds a Graduate Gemologist diploma from GIA and is a fellow of the Gemmological Association of Great Britain. She is the sixth recipient from GIA to win the award.

GIA Alumni Collective. The GIA Alumni Collective offers an exciting new networking platform for GIA graduates. The online community at collective.gia.edu allows a diverse group of users to access both live and self-paced continuing education seminars, join virtual chapters, connect with global alumni, and more. The site also puts GIA alums in the spotlight (figure 30), celebrating those who uphold the highest standards of GIA's consumer protection mission.

Deeta Thakural earned her Graduate Gemologist diploma at GIA's Mumbai campus. As a fourth-generation jeweler, Thakural was drawn to design. Her award-winning collections blend organic shapes and rich hues that reflect the natural world.

Mélanie Matthes studied at GIA's Carlsbad campus, receiving Graduate Gemologist, Pearls Graduate, and Applied Jewelry Professional diplomas. Her education, fascination with gemology, and love of history led to her career with a well-known auction house, handling some of the world's most extraordinary jewelry pieces.

Learning from GIA guided each member of the Hodge family down a different path. Aldis, a self-taught watchmaker and business owner, and his sister Briana, a visual specialist and photographer, encouraged their mother, Yolette, to explore her childhood fascination with diamonds and earn a Diamonds Graduate diploma.

Visit https://collective.gia.edu/meet-the-collective.html to read stories from these alumni and more.

***Gemmes*.** Swiss-based Gemmologie & Francophonie has launched a French-language digital publication, *Gemmes* (figure 31). Released twice a year, the magazine covers a range of gem and jewelry topics and is open to submissions. Each article has an English-language abstract and figure captions. The debut issue can be downloaded at gemmologie-francophonie.com/index.php/la-revue-gemmes. The second

Figure 30. Deeta Thakural, Mélanie Matthes, Yolette and Briana Hodge, and Aldis Hodge are some of GIA's featured graduates on the Alumni Collective website.

issue, available in September, will examine lab gemology, art history, ethics, and more.

CONFERENCE REPORTS

2023 Sinkankas Symposium. The Nineteenth Annual Sinkankas Symposium was held at GIA in Carlsbad, California, on April 22. Cohosted by GIA and the Geo-Literary Society, the event's theme was "San Diego County Gems and Minerals." Pink tourmaline, kunzite, spessartine garnet, and aquamarine were the focus of 11 presentations (figure 32).

Emcee **Robert Weldon** (GIA, Carlsbad) welcomed the capacity crowd to the first in-person Sinkankas Symposium since 2019. **Dr. Raquel Alonso-Perez** (Mineralogical and Geological Museum, Harvard University) recounted the history of the Pala Chief mine starting in the nineteenth century. **Bill Larson** and son **Will Larson** (Pala International, Fallbrook, California) examined the tourmalines of the Pala Gem Mining District and the Himalaya mine, respectively. **Brendan Laurs** (*Journal of Gemmology*) overviewed the geology of San Diego County pegmatites. **Nathan Renfro** (GIA,

Figure 31. The new French-language digital publication Gemmes, *published by Gemmologie & Francophonie.*

Figure 32. Brendan Laurs, Meg Berry, and Aaron Celestian at the Sinkankas Symposium. Photos by Judy Colbert.

Carlsbad) showed fascinating inclusion features of various gem minerals from the county. **Dr. Skip Simmons** (Maine Mineral and Gem Museum, Bethel, Maine) detailed the tourmaline mineral group's compositional variation, crystal structure, and classification.

Cal Graeber (Fallbrook, California) shared insights based on more than 50 years of experience mining and collecting San Diego County minerals. Lapidary artist **Meg Berry** (Megagem, Fallbrook, California) shared her decades of experience cutting locally mined tourmalines and showed several of her award-winning creations. By video, **Paula Crevoshay** (Albuquerque, New Mexico) looked back on her love affair with the gems of Southern California, which have often been incorporated into her acclaimed jewelry designs. **Dr. Aaron Celestian** (Natural History Museum of Los Angeles County) spoke on the use of gems to illuminate art and science. Using the museum's special exhibit of Crevoshay jewelry as an example, he explained its integration with social media and traditional print media to communicate scientific content. **Dr. George Rossman** (California Institute of Technology, Pasadena) joined **Dr. Aaron Palke** (GIA, Carlsbad) in examining the range of colors and color-causing elements in San Diego County gem minerals.

The next Sinkankas Symposium, scheduled for May 2024 in Carlsbad, will be on Burmese gems from Mogok.

Sustainability conference at JCK. GIA participated in two panels on sustainability during the June 2023 JCK Las Vegas show. President and CEO Susan Jacques started the first panel by sharing with the audience the United Nations Brundtland Commission's definition of sustainability: "Meeting the needs of the present without compromising the ability of future generations to meet their own needs." A discussion covering GIA's sustainability initiatives followed, highlighting the goal of building an inclusive and resilient future for people and the planet. These initiatives focus on social inclusion, environmental protection, and economic growth—all interconnected and crucial for the well-being of individuals and societies.

Sustainability has risen to the forefront of the gem and jewelry industry in the past ten years. A 2022 joint study by the Boston Consulting Group (BCG) and Comité Colbert estimated that 65% of consumers consider brands' sustainability commitment when purchasing luxury products, and McKinsey & Company projected that sustainability-influenced fine jewelry sales will go from 5–10% in 2019 to 20–30% in 2025.

GIA uses scientific and research-based expertise to advance its crucial consumer-protection mission by driving transparency and bringing clarity to sustainability in the gem and jewelry value chain. In June 2023, GIA released its first sustainability report, developed in reference to the Global Reporting Initiative (GRI) framework and to the institute's first sustainability strategy.

Looking ahead, GIA has outlined a sustainability strategy for the next two years. GIA's 2025 sustainability strategy outlines the organization's ambition for change, aiming to champion transparency by building resilience in the gem and jewelry sector through pioneering research and innovation, ultimately instilling greater confidence in GIA. The institute will drive change from the inside out by building an inclusive culture and reducing its climate impact. Drawing on a science-led approach, GIA plans to improve traceability through digital tools. Collectively, the institute will accelerate circularity, spearhead sustainability-related gemology research, and continue to raise awareness through responsible education programs. By working together to champion transparency and build all-important trust, GIA intends to spark real, sector-wide sustainable change.

The second panel gathered sustainability experts from across the industry: **Sara Yood** (Jewelers Vigilance Committee), **Iris Van der Veken** (Watch and Jewelry Initiative 2030), **Josephine Silla-Afuwape** (SCS Global Services), and consultant **Christina Miller**. The session began with various definitions of sustainability, followed by a discussion of how the industry collaborated on the Federal Trade Commission's Green Guides. Panelists analyzed rising sustainability regulations in Europe and the U.S. and changing consumer behaviors. The presentation ended with key initiatives needed to start a sustainability journey.

Johanna Levy
GIA, New York